Mon. Not. R. Astron. Soc. **000**, 1–9 (2006) Printed 5 February 2008 (MN LATEX style file v2.2)

The chemical content of nearby galaxies from planetary nebulae: NGC 147⋆

D. R. Gonçalves[1]†; L. Magrini[2]; P. Leisy[3,4] and R.L.M. Corradi[3,4]
[1] *IAG, Universidade de São Paulo, Rua do Matão 1226, 05508-900 São Paulo, Brazil*
[2] *INAF, Osservatorio Astrofisico di Arcetri, Largo E. Fermi, 5. I-50125, Firenze, Italy*
[3] *Isaac Newton Group of Telescopes, Apartado de Correos 321, E-38700 Sta. Cruz de La Palma, Spain*
[4] *Instituto de Astrofísica de Canarias, E-38205 La Laguna, Tenerife, Spain*

arXiv:astro-ph/0611756v1 24 Nov 2006

Accepted ?. Received ?; in original form ?

ABSTRACT

We report the results of spectroscopic observations, obtained with the GEMINI Multi-Object Spectrograph, of 8 planetary nebulae (PNe) in the dwarf spheroidal (dSph) galaxy NGC 147, a companion of M 31. The physico-chemical properties of the six brightest PNe (Corradi et. al. 2005) were derived using both the empirical ICF method and photoionization modelling with CLOUDY. Different aspects of the evolution of low and intermediate mass stars in a low-metallicity environment are analysed using relationships between chemical abundances. In addition, certain features of the chemical evolution of NGC 147 were examined. In particular, the mean metallicity of PNe, O/H=$8.06^{+0.09}_{-0.12}$ (corresponding to [Fe/H]$_{\rm PNe}\sim-0.97$), is close to the metallicity of the old stellar population, [Fe/H]=−1.0 (i.e. Butler & Martínez-Delgado 2005), suggesting a negligible chemical enrichment during a substantial amount of time. Finally, the luminosity-metallicity relationship for the dwarf galaxies of the Local Group is discussed. The location in the luminosity-metallicity diagram of dSphs does not exclude their formation from old dwarf irregular (dIrs) galaxies, but it does exclude their formation from the present time dIrs, since the differences between their metallicities are already present in their older populations. The offset in the luminosity-metallicity relationship indicates a faster enrichment of dSphs, and together with the different average abundance ratio [O/Fe] demonstrates the different star formation histories for these two types of galaxies.

Key words: Galaxies: abundances - Local Group - Individual (NGC 147)

1 INTRODUCTION

The rich variety of galaxies in the Local Group (LG) provides an opportunity to study in detail the formation and evolution of the most common types of galaxies in the Universe. One remarkable open question related to the evolution of dwarf galaxies is: are dwarf ellipticals and spheroidals the evolved descendants of previous star-forming dwarfs? This hypothesis can be tested through the metallicity-luminosity relation for LG dwarfs (Skillman et al. 1989). The key problem with this relation is that there are large uncertainties in the [O/Fe] assumed for non star-forming galaxies (Richer & McCall 1995). A way to address this problem is by deriving the chemical abundances of a significant sample of LG dwarf galaxies using emission-line objects, such as PNe, which are present from early- to late-type galaxies. In fact PNe and H II regions have been used to address this issue by a few groups (Richer & McCall 1995; Stasinska, Richer & McCall 1998; Magrini et al. 2005). Our motivation for this paper is to contribute to such a study by discussing new spectroscopic data for NGC 147 from the GEMINI telescope.

NGC 147, together with NGC 205 and NGC 185, is one of the three brightest dwarf companions of M31. At variance with NGC 185, NGC 147 is gas and dust free. The amount of H I in NGC 205 and NGC 185 is significantly higher than in NGC 147, in which the H I column density is at least a factor of 10 lower than in the other two galaxies. The dust clouds that are prominent in NGC 205 and NGC 185 are also lacking in NGC 147 (Young & Lo 1997). NGC 147 and NGC 185 have similar star formation histories and are dominated by their old stellar populations, while NGC 205

⋆ Based on observations obtained at the Gemini Observatory, which is operated by the Association of Universities for Research in Astronomy, Inc., under a cooperative agreement with the NSF on behalf of the Gemini partnership.

† E-mail: denise@astro.iag.usp.br

shows several peculiarities, including a younger population (Mateo 1998).

The stellar metallicity of NGC 147 is relatively well known. Based on deep V and I photometry of the central regions, Davidge (1994) has shown that NGC 147 is moderately metal-poor ([Fe/H]=−1±0.3). Its colour-magnitude diagram indicates the presence of old red giant branch (RGB) stars, as well as some stars formed at intermediate epochs, like asymptotic giant branch (AGB) stars about 5 Gyr old. Using RGB colours, Han et al. (1997) give two slightly different metallicities for the inner (up to 1.5′ from the centre) and outer (from 1.5 to 4′) fields of the galaxy, namely −0.91 and −1.0, respectively. They point out that there is a weak tendency of increasing metallicity with galactocentric radius in the outer field. Han et al. (1997) also stress the presence of an AGB population with an age of several Gyrs, and the absence of main sequence stars with M_V <1, suggesting that the star formation in NGC 147 ceased at least 1 Gyr ago. On the other hand, Nowotny et al. (2003) used a four-colour photometry to analyse the late-type stellar content of this galaxy and that of NGC 185, separating AGB stars of different chemistry (O- and C-rich, i.e., M- and C-type stars). From the mean RGB colour indices, they conclude that the metallicity of NGC 147 is [Fe/H]=−1.11 and that of NGC 185 is [Fe/H]=−0.89.

In summary, following the above arguments and the work by Mateo (1998), while NGC 147 and NGC 185 are very similar in terms of their stellar content, star formation history and absolute luminosity, their metallicity is different.

In this paper, we present the determination of chemical abundances in NCG 147 using PNe. These data allow us to address some aspects of the chemical evolution of the galaxy, its consequences for the luminosity-metallicity relation of the LG dwarfs, as well as the properties of the PNe themselves. In fact, it appears that NGC 147 and NGC 185 also have different PNe populations: PNe in NGC 185 are systematically brighter than those in NGC 147 (Corradi et. al. 2005). Note that lower limits for the O/H abundances of the PNe in NGC 185 and NGC 205 were determined by Richer & McCall (1995).

The paper is organized as follows. The Multi Object Spectroscopy (MOS) data and their reduction are discussed in Section 2. In Section 3, we present the derivation and analysis of the PNe physical parameters and chemical abundances. These are then discussed in Sect. 4 using different relationships, and in Sect. 5 they are compared with the stellar metallicity and the age-metallicity relation. Section 6 is devoted to the luminosity-metallicity relation for dwarf spheroidals and irregulars. Finally, our conclusions are presented in Section 7.

2 DATA ACQUISITION AND REDUCTION

Seven of the nine PNe identified in NGC 147 from narrow band photometry by Corradi et. al. (2005) were observed spectroscopically using the GEMINI Multi-Object Spectrograph North (GMOS-N).

The pre-imaging needed to build the MOS mask was also obtained with GMOS-N on August 14, 2005. Images were taken using a narrow-band Hα filter and a broad-band continuum filter R, whose central λ and $\Delta\lambda$ are 655/6.9nm and 657/83nm, respectively. The exposure times were 2×300s in Hα and 2×60s in R. The seeing was <0.7 arcsec. These images were used to produce a continuum-subtracted image to determine the position of the long-slits and to create a MOS mask containing seven PNe. In addition, a new PN was identified with the GMOS pre-imaging and consequently inserted in the spectroscopic observations. The identification of the original 7 PNe in the MOS mask are those given by Corradi et. al. (2005) in their Table 1, and named PN1 to PN7. The coordinates of the new PN, called PN 10, are: R.A.=00 33 11.87, Dec=+48 28 11.7 (J2000.0). Figure 1 shows the image of NGC 147, marking the position of the 8 PNe studied in this work.

The GMOS-N in its spectroscopic mode was used in two different nights to obtain the PN spectra. The "red" spectra were taken on October 31, 2005 with the R400+5305 grating, in two exposures of 1800s each. As for the "blue" spectra, data were obtained on December 3, 2005, with the B600+G5303 grating, in 2×2800s exposures. In both configurations the slits widths were 1 arcsec, and the pixel binning was 2×2 (spectral×spatial). The spectral and spatial resolutions were: 0.3 nm and $0''.094$ pix^{-1}, respectively, with B600 and 0.8 nm and $0.''134$ pix^{-1} with R400. The seeing during the "blue" and "red" spectroscopic observations was <0.5 arcsec and <0.7 arcsec, respectively.

A CuAr calibration was obtained with the B600+G5303 grating, but the only CuAr exposure taken with R400+5305 was not good enough to be used for wavelength calibration. Because of that, we have calibrated all the "red" spectra using a list of skylines. This method gives a satisfactory wavelength calibration, thanks to the large number of skylines in the red part of the spectra. An exposure of the spectroscopic standard star G191B2B was taken with each configuration around the date of the observation of the spectra, and these exposures were applied in the flux calibration of our data. Data were reduced using the GEMINI GMOS DATA REDUCTION SCRIPT and LONGSLIT tasks, both being part of the IRAF package.

The selected slit length varies from one PN to another according to the field crowdedness. Also, different slit distances from the bisector of the mask in the North-South direction correspond to a different wavelength coverage. Typically, the "blue" spectra covered a spectral range from 300–350 nm to 570–650 nm. In the case of the "red" spectra, they covered from 500-620 nm to 920–1050 nm. Note that there is some wavelength overlap between the "blue" and "red" spectra. As an intense emission line was not always found in the overlap zone, we used the spectra of PN3 which contains the Hα line in both "red" and "blue" spectra to obtain a scale factor of 0.8 for all PNe. This scale factor was applied to the fluxes measured in the "red" spectra in order to get the fluxes reported in Table 1. In fact, from our previous experience with multi-object spectroscopy, we have noticed that differences of the scale factors are generally small, amounting to about 5-10%. We have also evaluated which is the error that we are adding to the measured fluxes due to the uncertainty in the matching. This error amounts to about 7%, which can be considered a characteristic measure of the uncertainty on the scale factors.

Note that in PN5 only the fluxes of the [O III] 495.9 nm and 500.7 nm lines were measured, so that this PN does not appear in the following analysis. Errors in the fluxes

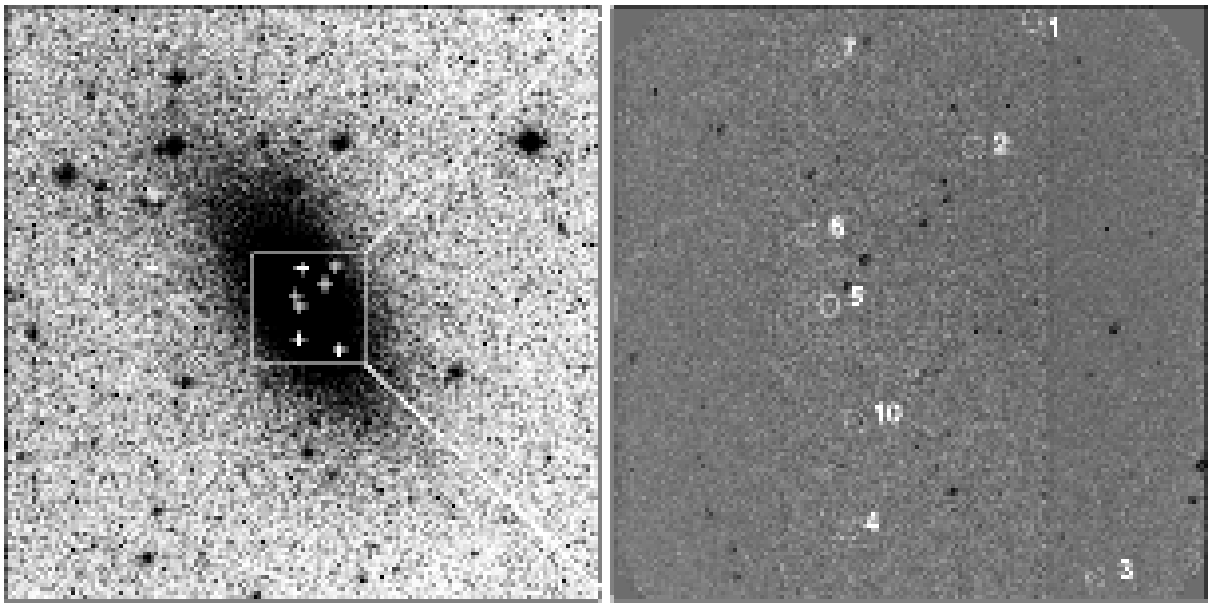

Figure 1. *Left*: The $34' \times 34'$ Digitalized Sky Survey image centred in NGC 147. Plus signs mark the position of the PNe candidates studied by Corradi et. al. (2005). *Right*: The $5.5' \times 5.5'$ GMOS-N continuum-subtracted, Hα-R, image of NGC 147, with circles marking the position of the 8 PNe contained in the MOS mask. See text and Table 1 of Corradi et. al. (2005) for the RA and DEC of the PNe.

were calculated taking into account the statistical error in the measurement of the fluxes, as well as systematic errors of the flux calibrations, background determination, and sky subtraction. Table 2 shows the estimated percentage errors for a range of line fluxes (relative to Hβ=100) in each PN. Here, and throughout the paper, quoted uncertainties are 1-σ errors.

3 DATA ANALYSIS

3.1 Extinction and Physical Parameters

The observed line fluxes were corrected for the effect of the interstellar extinction using the extinction law by Mathis (1990) with R_V=3.1. We used c_β as a measurement of the extinction, which is defined as the logarithmic difference between the observed and de-reddened Hβ fluxes. Since the "blue" part of the spectra, which contains also the Hδ and Hγ lines, is affected by larger uncertainties, the c_β was determined comparing only the observed Balmer I(Hα)/I(Hβ) ratio with its theoretical value, 2.85 (Osterbrock 1989). For the higher signal to noise spectrum of PN4, whose Hβ line was lost in the gap between two CCDs, the I(Hα)/I(Hγ) was used to compute the extinction. The values of c_β and their 1-σ errors are shown in the last row of Table 1. c_β is related to E(B-V) through the following relation: c_β=0.4 R$_\beta$ E(B-V), where R$_\beta$=3.7. The average value of the extinction of the PNe $<c_\beta>$=0.07±0.07 gives E(B-V)=0.05±0.10, which is comparable with the reddening value E(B-V)=0.173 derived by Schlegel, Finkbeiner & Davis (1998) toward NGC 147, from dust infrared emission features. Patchiness of dust and gas toward NGC 147 (Sohn et al. 2006) might be the reason of appreciable variations of the reddening throughout the galaxy area.

The extinction-corrected intensities (given in the middle column of Table 1) were then used in order to obtain the densities and temperatures for each PN. As we can see in Table 1, [S II]$\lambda\lambda$671.6,673.1, usually used as an electron density estimator, was measured only in PN4, PN6 and PN10 (and an upper limit is given for PN1). As for the temperature estimation, we were able to use the I(λ495.9+λ500.7)/I(λ436.3) ratio, giving T_e[O III], for all the PNe but PN10 (also note that only an upper limit is given for PN6). In the particular case of PN4, two other temperature estimators were also used, namely I(λ654.8+λ658.3)/I(λ575.5) for T_e[N II] and I(λ372.6+λ372.9)/I(λ732.0+733.0) for T_e[O II]. The derived electron densities and temperatures, and their errors, are listed in the upper part of Table 3.

This is the first direct determination of the physical parameters of emission line objects in NGC 147, which prevents us to perform any external comparison.

3.2 Empirical ICF abundances

Chemical abundances were derived from the emission-line intensities using the Ionization Correction Factors (ICF) method. The ICF were computed following the prescriptions by Kingsburgh & Barlow (1994).

As mentioned above, the [O III] 436.3 nm emission line was measured with a sufficiently high signal to noise ratio in five PNe, namely PN1, 2, 3, 4, and 7. There, T_e[O III] could be directly determined. In one case, PN6, we could estimate an upper limit to the [O III] 436.3 nm emission line, and consequently an upper limit to T_e[O III].

For PN 10, we could not measure this temperature diagnostic emission line, and therefore we could not derive its chemical abundances. Finally, as noted before, in the spectrum of PN5, only the [O III] doublet 495.9,500.7 nm could be detected, preventing any further analysis. In PN4, T_e[O III] was used in computing chemical abundances with the

ICF method for ions which are ionized twice or more times, and T_e[N II] for singly ionized species.

The ICF method was applied to the six PNe with an electron temperature measurement. Formal errors on the ICF abundances were computed taking into account the uncertainties in the observed fluxes, in the electron temperatures and density, and in the c_β, as done in Gonçalves et al. (2003) and Magrini et al. (2005). The ionic and total abundances, as well as the ionization correction factors, are reported in Table 4.

3.3 CLOUDY photoionization modelling

PNe were also modelled using the photoionization code CLOUDY 95.06 (Ferland et al. 1998). The complete procedure is described in Magrini et al. (2004). Here we remind the most important parameters and assumptions. The input parameters for CLOUDY are *i*) the energy distribution, *ii*) the luminosity of the central star, *iii*) the nebular geometry, *iv*) the hydrogen density, N_H, and *v*) the chemical abundances. At the large distance of NGC 147, PNe are not resolved and we assumed the most simple geometry of spherical symmetry with constant density. The energy distribution of the central star was set to that of a blackbody (BB). In fact, as described by Magrini et al. (2004), the model atmospheres by Rauch (2003) give similar results in terms of chemical abundance determinations. Dust grains were added to the models, since they have an important effect, particularly on the temperature structure of the PNe (see, for instance, Gonçalves et al. 2004). This effect depends on the type of grain (graphite and/or silicate), the grain abundances, and the grain-size distribution, being more relevant in the inner regions of the nebula (see Dopita & Sutherland 2000). Dust type and size distribution adopted are those typical of Galactic PNe, with ISM gas-phase depletion due to grains following van Hoof et al. (2004).

The BB temperature $T_\star$ was derived using Ambartsumian's method (Ambartsumian 1932), i.e. using the HeII(λ468.6)/HI(λ486.1) line flux ratio, or the ([OIII]λ495.9+[OIII]λ500.7)/HeIIλ468.6 line ratio method (Gurzadyan 1988). This is done only for the first iteration, in the following ones the BB temperature was adjusted as to match the HeI/HeII line ratio.

The luminosity $L_\star$ of the central star was set to reproduce the photometric absolute flux of the [O III] λ500.7 nebular line, as given in Corradi et. al. (2005). The external and internal radii of the shell, R_{in} and R_{ext}, were varied to match the ratio of lower and higher excitation ions, as [O III]/[O II]. Density was derived from the [S II] λ671.7/λ673.1 intensity ratio, which was measured in PN1, PN4, and PN6. For the remaining PNe, it was assumed to be equal to 5000 cm^{-3}, which can be considered a typical value for Galactic PNe (see e.g. Stanghellini & Kaler 1989). In addition, we made some tests varying the density by $\pm$1000 cm^{-3} with both the ICF and CLOUDY methods, obtaining negligible changes in the computed abundances. We assumed the average non-Type I Galactic PNe abundances from Kingsburgh & Barlow (1994) as initial chemical abundances. The parameters of the best CLOUDY model (for the central star $T_\star$, $L_\star$, and for the nebula N_H, R_{in}, R_{ext}) are shown in the second half of Table 3.

Subsequently, chemical abundances were varied to match the observed and predicted intensities within 5% for the lines brighter than Hβ and 10% for the other lines. As explained above, we considered dust in our modeling. This inclusion came from the necessity of finding a good agreement between the empirical and CLOUDY temperatures. The abundances of C, O and Fe (the most important coolants) were also slightly modified to refine the match with the empirical T_e. It is clear from Table 3 that the model T_e is similar to the empirical one, with the exception of PN4. In the latter case, we have three different empirical measurements of the electron temperature. Our simple model with uniform density is not capable of reproducing the empirical temperatures, likely because of different conditions in different zones of the nebula. We therefore decided to reproduce just the the average of T_e[O III] and T_e[N II]. No other simple assumption for the N_e radial profile (e.g. decreasing with radius) was able to reproduce satisfactorily the observed line intensities.

The results of the best-fitting CLOUDY models, in terms of chemical abundances (and their errors) are shown in Table 5. Note that ICF abundances are in good agreement with those derived using CLOUDY, whose mean values for the different elements, in units of 12 + log X/H, are: He/H=$11.02^{+0.20}_{-0.36}$; O/H=$8.06^{+0.09}_{-0.12}$; N/H=$7.70^{+0.18}_{-0.31}$; Ne/H=$6.68^{+0.18}_{-0.32}$; S/H=$6.35^{+0.25}_{-0.68}$; and Ar/H=$5.13^{+0.24}_{-0.64}$.

4 CHEMICAL ABUNDANCE PATTERNS

PNe are formed by stars ranging from 0.8 to 8 $M_\odot$, which loose their chemically enriched envelopes during the AGB evolution. Relationships between chemical abundances of He/H, N/O, N/H and O/H are known to exist in Galactic PNe (cf. Henry 1990). Extragalactic PNe are important because they allow us to test if these relationships also hold in different environments. In particular, PNe belonging to dwarf galaxies permit to extend these relations to very low metallicities.

The relation between log N/O and He/H for the PNe of NGC 147 (except PN3, for which only a crude limit of N/H could be derived) is shown in Figure 2, where our CLOUDY chemical abundances are compared with the models by Marigo (2001), built for initial metallicities of Z=0.008, and new models by Marigo (private communication) for Z=0.001 and Z=0.004. The lower metallicity models (Z=0.001 and Z=0.004) predict, for progenitor masses below 3$M_\odot$, an enhancement of O/H compared to N/H, producing a N/O abundance ratio that decreases with He/H. For higher mass progenitors, N/O increases quickly and significantly as the result of hot-bottom burning. In the model with Z=0.008, the N/O ratio remains almost constant for initial masses below 3$M_\odot$. The metallicity of NGC 147 is Z=0.002 (cf. Davidge 1994; Han et al. 1997; Nowotny et al. 2003). Taking into account the errors of the He abundances and of the N/O ratio, the NGC 147 PNe are consistent with the Z=0.001 and Z=0.004 tracks. PN4 and PN7 might be consistent with a higher metallicity, and consequently a more recent formation.

The correlation between log N/O and 12 + log N/H is shown in Figure 3 for PNe belonging to several LG galaxies. This relation is well defined for PNe with a slope close to unity, suggesting that the increase of N/O with N/H is due

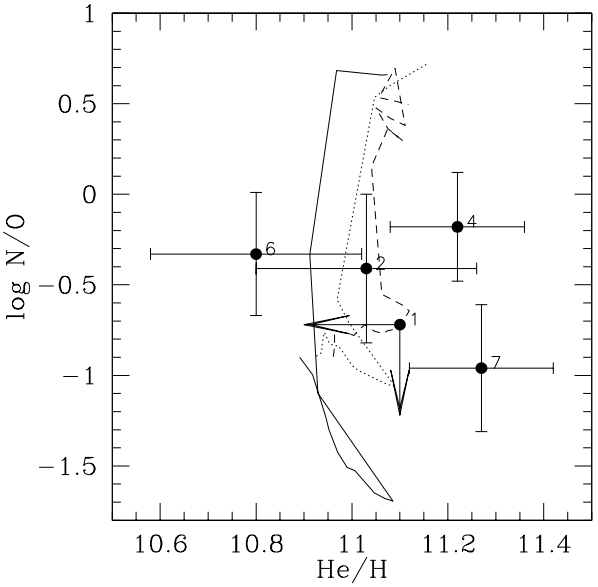

Figure 2. The relationship between log N/O and He/H. The solid (Z=0.001) and dotted (Z=0.004) lines represent the stellar models for the progenitors (Marigo 2004, private communication), and the dashed line is the model with Z=0.008 (Marigo 2001). Filled circles correspond to NGC 147 PNe with CLOUDY He/H and N/O abundances.

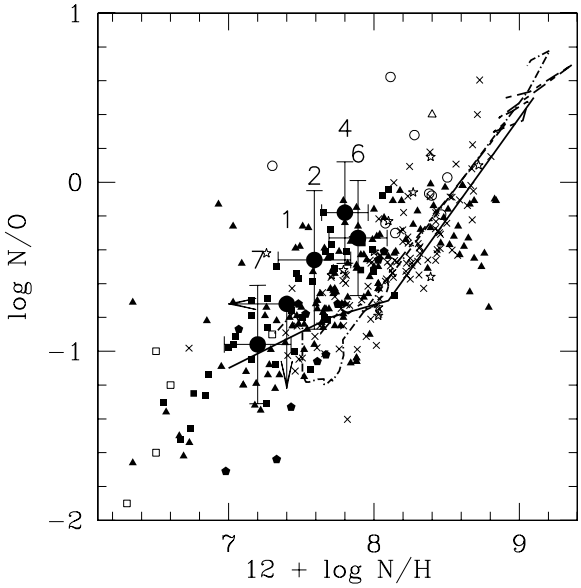

Figure 3. The relationship between log N/O and 12 + log N/H for LG PNe. The dash-dotted line is the model by Groenewegen & de Jong (1994) for the LMC metallicity and initial masses from 0.93 (left) to 8.5 $M_{\odot}$(right). The solid line indicates the model for Z=0.004 and the dashed line that for Z=0.008. Both models are for initial masses from 0.8 (left) to 5 $M_{\odot}$(right) (Marigo 2001). The CLOUDY abundances of NGC147 PNe are marked with filled circles. Observed abundances are from: Galaxy (crosses, Perinotto, Morbidelli & Scatarzi 2004); LMC and SMC (filled triangle and squares, respectively, Leisy & Dennefeld 2006); M31 (stars, Jacoby & Ciardullo 1999); M33 (filled pentagons, Magrini et al. 2004); Sextans A and B (empty triangle and squares, Magrini et al. 2005); M32 (empty circles, Richer et al. 1999).

to the increase of N, which is mainly produced by the CN cycle, without modifying the oxygen abundance through the ON cycle. Theoretical predictions of N/O vs. N/H for different masses of the progenitor stars and metallicity (Groenewegen & de Jong 1994, for the LMC metallicity; and Marigo 2001; for Z=0.001 and Z=0.004) are also shown. Note that Type I PNe which experienced hot bottom burning conversion of C to N, are located outside the relation. The PNe of NGC 147 are in agreement with the general behaviour of the LG PNe. Following the classical definitions of Galactic Type I PNe, N/O$\geqslant-0.3$ and He/H$\geqslant$11.1 (Peimbert & Torres-Peimbert 1983) or the more stringent one N/O>-0.1 (Kingsburgh & Barlow 1994), the NGC 147 sample does not include Type I PNe. However, it has to be noted that the original definition of Type I PNe only holds for the metallicity of the Galaxy (Magrini et al. 2004). The absence of Type I PNe would not be surprising if we consider that they are typically associated to younger progenitors (Corradi & Schwarz 1995) while the predominant stellar population in this galaxy is very old.

Figure 4 shows the log O/H vs. 12 + log N/O for a sample of LG PNe. There is not a clear correlation between these two quantities, as already noted in previous works (cf. Henry 1990; Richer 2006).

5 THE CHEMICAL EVOLUTION OF NGC 147

The elemental abundances shown in Table 4 and Table 5 can also be compared with the metallicity measured in stars of this galaxy. Given that ICF and CLOUDY abundances are in good agreement, we use the CLOUDY O/H mean value, as given in the last row of Table 5, that considers six PNe.

In principle, O/H can be converted into [Fe/H] using the following relation: $[Fe/H]_{PNe}=[O/H]_{PNe}-0.37$ obtained by Mateo (1998). This relation is useful for comparing samples of galaxies, but less valid considering galaxies individually. Even on a statistical sense, this transformation is uncertain ($\pm$0.06 dex; Mateo 1998). Keeping in mind this strong limitation, the mean O/H that we obtained for NGC 147, gives $[Fe/H]_{PNe}=-0.97$ ($[O/H_{solar}=8.66$; Asplund 2003), in agreement with metallicities of the RGB population (Davidge 1994; Han et al. 1997; Nowotny et al. 2003), discussed in Sect. 1. Moreover, when we plot $[Fe/H]_{PNe}$ in terms of the galactocentric distance (not shown here), the weak gradient with metallicities increasing from the central to the outer zones of the galaxy, argued by Han et al. (1997), is not confirmed. In summary, this crude agreement between PNe metallicities and old-population metallicity would suggest that NGC 147 did not experience a significant chemical enrichment during a long period of time.

As described in Section 3.3, the modelling with CLOUDY allowed us to estimate stellar parameters as the luminosity and temperature of the central stars. The model $T_{\star}$ and $L_{\star}$ are listed in Table 4 and can be located in the $\log T_{\star}$-$\log L_{\star}$ diagram. Their location are then compared with the available H-burning and He-burning evolutionary tracks, for Z=0.004 and Z=0.001 (Vassiliadis & Wood 1994), as shown in Figure 5. From the loci of the central stars in the H-R diagram, we can estimate the central star masses, which range

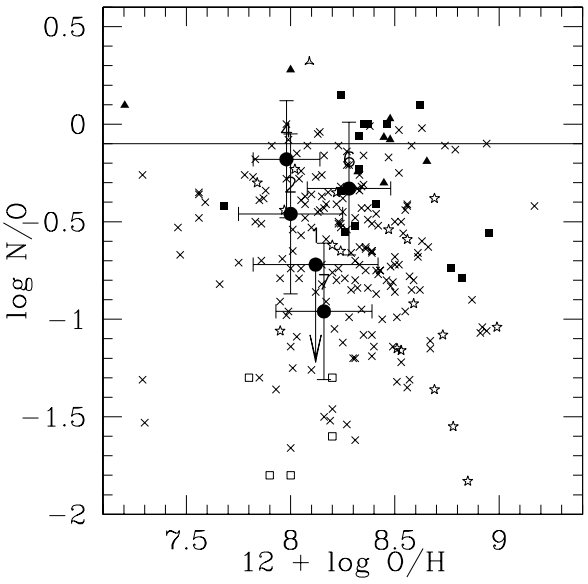

Figure 4. log O/H vs. 12 + log N/O. CLOUDY abundances of the PNe in NGC 147 are marked with circles. Observed abundances are from: M31 bulge (filled squares, Jacoby & Ciardullo 1999); M33 (empty stars, Magrini et al. 2004); Magellanic Clouds (crosses, Leisy & Dennefeld 2006); M32 (filled triangles, Richer et al. 1999); Sextans A and B (empty triangle and squares, Magrini et al. 2005); LeoA (cross, Van Zee et al. 2006).

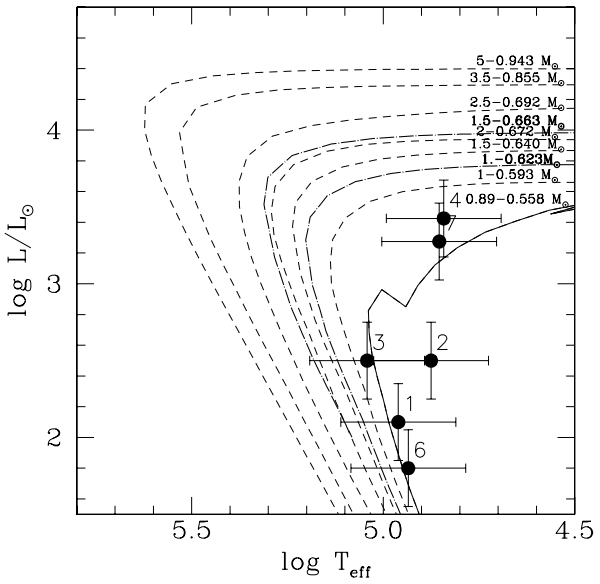

Figure 5. The H-R diagram of the PNe central stars. Luminosities and temperatures were derived with the CLOUDY photoionization models. The evolutionary tracks are by Vassiliadis & Wood (1994): Z=0.004 continuous lines and Z=0.001 dashed lines.

from 0.56 to 0.59 $M_\odot$. Using the initial to final mass relationship adopted by Vassiliadis & Wood (1994), we find that the masses of the progenitor stars were between 0.9 and 1.0 $M_\odot$. Stars with these main sequence masses and with an initial metallicity of Z=0.001 were born about 10 to 7 Gyr ago (Charbonnel et al. 1999). This is in agreement with what is known about the star formation history of NGC 147. As described in Sect. 1, the colour-magnitude diagrams suggest the presence of old RGB stars and of a small number of intermediate-age AGB stars with an age of about 5 Gyr.

From the study of chemical evolution of dwarf spheroidal galaxies, it is known that these galaxies are characterized by one or two long bursts of star formation (Lanfranchi & Matteucci 2003). The low gas content is the result of gas consumption by star formation and gas removal by an efficient galactic wind.

A detailed comparison of the PNe abundances obtained in this paper with those for the other two bright dwarf companions of M31 is not possible. The only other available PNe study for these galaxies is in fact that of Richer & McCall (1995), who have observed only two PNe in NGC 205, one of them giving 12 + log O/H=8.21 and the other $\geqslant$ 8.11. In the case of NGC 185 (Richer & McCall 1995), the [O III]4363 nm line was not detected in any of the PNe, thus the derived abundances are quite uncertain. Richer & McCall (1995) applied empirical methods, derived from properties of PNe in the Magellanic Clouds and the Milk Way, to correct their lower limits of O/H, concluding that their values underestimate the O/H abundances of these two galaxies by 0.37 dex. After this correction, they obtained 12 log O/H=8.60 and 8.20 for NGC 205 and NGC 185, respectively, which are comparable to the value of $8.06^{+0.09}_{-0.12}$ that we find for NGC 147 (within the uncertainties).

6 THE LUMINOSITY-METALLICITY RELATIONSHIP OF dIrs AND dSphs

It has been proposed that dwarf spheroidal galaxies are formed through the removal of the gas in dwarf irregulars, either through ram pressure stripping, supernova driven winds or star formation (Kormendy & Djorgovski 1989). In this scenario, as described by Richer & McCall (1995), once the gas finished and the star formation stopped, the old dIr-like galaxies fade in luminosity as their stellar population ages. According to this, dSphs are expected to have, at a given luminosity, a higher metallicity than dIrs. The luminosity-metallicity relationship has been deeply studied for dIr galaxies by several authors (Skillman et al. 1989; Richer & McCall 1995; Larsen et al. 2001; Van Zee et al. 2006; Lee et al. 2006). One of the most recent compilation of oxygen abundance in nearby low luminosity gas rich galaxies, dIrs, is by Van Zee et al. (2006). The weighted least-squares fit to the luminosity vs. metallicity data for the fifty dIr galaxies within 50 Mpc with an oxygen abundance determination is

$$12 + \log(O/H) = 5.67 - 0.151 M_B. \quad (1)$$

While oxygen abundances can be derived relatively easily for gas rich galaxies using H II regions, it is quite difficult to obtain them for non-star forming dSph galaxies. On the other hand, for these galaxies the stellar iron abundances are known. The comparison of dSph metallicity with dIr oxygen abundances is thus dependent on the [O/Fe] adopted. This ratio depends in turn on the star formation history (Gilmore & Wyse 1991). To overcome the problem,

Richer & McCall (1995) proposed to use PNe as probes of the stellar oxygen abundance in both dIrs and dSphs. PNe are in fact present in all types of galaxies and, with few exceptions Magrini et al. (2005, cf. Sextans A PNe), they do not produce oxygen, and thus they are representative of the stellar progenitor oxygen abundance.

Figure 6 shows the luminosity-metallicity relationship obtained using oxygen abundances of H II regions. the continuous line is the fit by Van Zee et al. (2006). The oxygen abundances of PNe in dIrs are marked with stars and those of PNe in dSphs with filled circles. The average oxygen abundance of PNe in NGC 147 is marked with a filled square. Note that the dIr PNe abundances are in good agreement with the luminosity-metallicity relation from H II regions, with the exception of the only PN of Sextans A, where oxygen dredge-up occurred (see Magrini et al. 2005). On the other hand, the oxygen abundances of dSph PNe exceed those predicted by eq. 1: at a given luminosity, dSphs have a higher metallicity than dIrs.

The similarity of the oxygen abundance found in PNe belonging to dIr galaxies to that found in the ISM (H II regions) suggests that the observed PNe in dIrs, which are also the brightest, are the products of rather recent star formation. At variance, the mean abundance in the PN population of dSph galaxies, where star formation ceased long ago, should be closer to the mean abundance of the stellar populations in that galaxy. Considering, thus, the difference of the age of the PN populations in dIrs and dSphs, the true difference between the oxygen abundances referred to the same epoch in dwarf irregulars and spheroidals might be larger than what Figure 6 indicates. The offset in the luminosity-metallicity diagram does not rule out the possibility that dSph galaxies come from primordial dIrs-like progenitors that consumed all their gas content and then faded in luminosity (cf. Richer & McCall 1995). On the other hand, the metallicity offset is against the hypothesis that dwarf spheroidals form from present-time dwarf irregulars. As discussed by Grebel (2005), dwarf irregulars and dwarf spheroidals may have been very similar initially, but the early evolution of the two types differed greatly, with dwarf spheroidals forming more stars and enriching themselves more, as observed from their stellar population –which is more metal rich than those of dIrs.

If we also consider the [O/Fe] ratio, as discussed extensively by Richer & McCall (1995), large differences of this ratio in dIrs and dSphs are found (see their Table 6). [O/Fe] is larger in dSphs than in dIrs, reflecting the higher gas consumption rate of the dSphs and therefore a substantially different star formation history. The [O/Fe]=0.44 of NGC 147, computed adopting [Fe/H]=-1 by Davidge (1994) and solar abundances of iron and oxygen by Asplund (2003), point in this direction.

In conclusion, the offset in the luminosity-metallicity relationship indicates a faster enrichment of dSphs, and together with the different average abundance ratios [O/Fe] highlights different star formation histories for these two classes of galaxies.

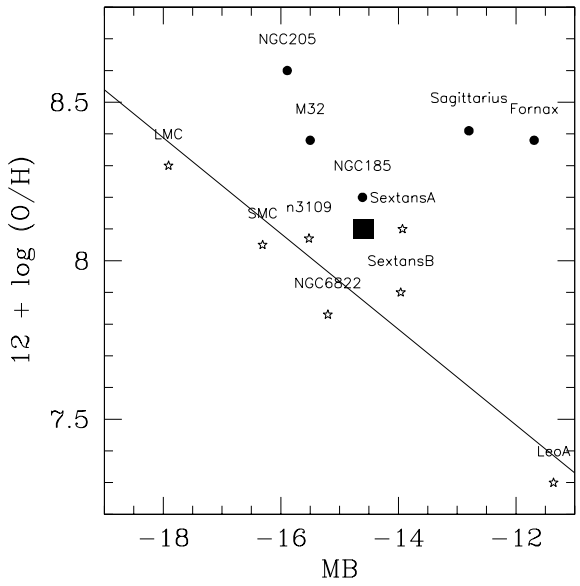

Figure 6. Luminosity-metallicity for dwarf galaxies in the LG. dSphs are marked with filled circles, dIrs with stars, NGC 147 average abundance with a filled square. Abundances determinations: NGC 147 (this work), LMC and SMC (Leisy & Dennefeld 2006), Sextans A and B (Magrini et al. 2005), NGC 205, NGC 185, Fornax (Richer & McCall 1995), Sagittarius (Zijlstra et al. 2006), Leo A (Van Zee et al. 2006), M32 (Stasinska, Richer & McCall 1998), NGC 6822, NGC 3109 (Leisy et al., in prep.). The almost diagonal line marks the luminosity-metallicity relation obtained from H II regions (Van Zee et al. 2006).

7 CONCLUSIONS

Using the ICF method as well as CLOUDY photoionization modelling, we have analyzed new GEMINI MOS data for the PNe of NGC 147, one of the most remarkable dwarf spheroidal companions of Andromeda. The physical parameters and the elemental abundances of He, O, N, Ne, Ar and S, for the six brightest PNe identified in this galaxy by Corradi et. al. (2005) have been determined.

We find that, adopting the definition in the Galaxy, there are no Type I PNe in the NGC 147, an expected result, since Type I PNe are typically associated to younger and massive progenitors, while the predominant stellar population in this galaxy is old.

From the literature, the comparison of the near-IR photometry of the AGB stars in the three brightest M31 dwarf companions shows that ages of 1 and 0.1 Gyr are predicted for the most recent star formation in NGC 185 and NGC 205, respectively, while the last event that formed stars in NGC 147 occurred some 1 to 3 Gyr ago (Davidge 2005; Han et al. 1997). In terms of the stellar metallicity, the three galaxies have similar median photometric abundances: [Fe/H]=-1.11±0.08 (NGC 185); -1.06±0.04 (NGC 205); and -1±0.03 (NGC 147) (Butler & Martínez-Delgado 2005).

Our determination of the oxygen abundance for the PNe of NGC 147, is comparable (within the uncertainties) to those of NGC 185 and NGC 205. The O/H abundance converts to $[Fe/H]_{PNe}$=-0.97, which is similar to the stellar metallicity of NGC 147. This similarity between

intermediate-age PNe population and the old stellar population of the galaxy implies that no significant chemical enrichment has occurred during a long period of time.

Finally, the luminosity-metallicity for the dwarf galaxies of the Local Group is analyzed. We conclude that the location in the luminosity-metallicity diagram of dSphs exclude their formation from present-time dIrs, and together with the abundance ratio [O/Fe] points to different star formation histories for these two classes of galaxies.

ACKNOWLEDGMENTS

We would like to thank M. Richer, the referee of this paper, for his valuable comments and suggestions which significantly improved the paper. We acknowledge M. Perinotto for using his program to perform a fast evaluation of the chemical abundances that we then compared with our own evaluation. The work of DRG is supported by the Brazilian Agency FAPESP (03/09692-0 and 04/11837-0), and that of LM by the Italian National Institute of Astrophysiscs (INAF).

REFERENCES

Ambartsumian V. A., 1932, Poulkovo Obs. Circ 4, 8
Asplund M., 2003, CNO in the Universe, ed. C. Charbonnel, D. Schaerer, & G. Meynet (San Francisco: ASP), ASP Conf. Ser., 304, 275
Butler D. J., & Martínez-Delgado D., 2005, AJ, 129, 2217
Charbonnel C, Dappen W., Schaerer D., Bernasconi P. A., Maeder A., Meynet G., Mowlavi N., 1999, A&AS, 135, 405
Corradi R. L. M., & Schwarz H. E., 1995, A&A, 293, 871
Corradi R. L. M., et al., 2005, A&A, 431, 555
Davidge T. J., 1994, AJ, 108, 2123
Davidge T. J., 2005, AJ, 130, 2087
Dopita M. A., & Sutherland R. S., 2000, ApJ, 539, 742
Ferland G. J., Korista K. T., Verner D. A., Ferguson J. W., Kingdon J. B., & Verner E. M., 1998, PASP 110, 761
Gilmore G., & Wyse R. F., 1991,ApJ, 367,L55
Gonçalves D. R., Corradi R. L. M., Mampaso A., & Perinotto M., 2003, ApJ, 597, 975
Gonçalves D. R., Mampaso A., Corradi R. L. M., Perinotto M., Riera A., López-Martín L., 2004, MNRAS, 355, 37
Grebel, E. K. 2005, in Stellar Astrophysics with the World's Largest Telescopes: First International Workshop on Stellar Astrophysics with the World's Largest Telescopes, ed. J. Mikolajewska and A. Olech (New York: American Institute of Physics), AIP Conference Proceedings, 752, 161
Groenewegen M. A. T., & de Jong T., 1994, A&A, 282, 127
Gurzadyan G. A., 1988, ApSS, 149, 343
Han M., Hoessel J. G., Gallagher, J. S. III, Holtsman J., Stetson P. B., 1997, AJ 113, 1001
Henry R. B. C., 1990, ApJ, 356, 229
Kingsburgh R. L., & Barlow M. J., 1994, MNRAS 271, 257
Kormendy J, & Djorgovski S., 1989, ARA&A, 27, 235
Jacoby G. H., Ciardullo R,, 1999, ApJ, 515, 169
Lanfranchi G. A., Matteucci F., 2003, MNRAS, 345, 71
Larsen T. I., Sommer-Larsen J., Pagel B. E. J., 2001, MNRAS, 3223, 555
Lee H., Skillman E. D., Cannon J. M., Jackson D. C., Gehrz R. D., Polomski E. F., Woodward C. E., 2006, ApJ, 647, 970
Leisy P. & Dennefeld M., 2006, A&A, 456, 451

Magrini L., Perinotto M., Mampaso A. & Corradi R. M. L., 2004, A&A 426, 779
Magrini L. Leisy P., Corradi R. M. L., Perinotto M., Mampaso A. & Vílchez J. M., 2005, A&A 443, 115
Marigo P., 2001, A&A, 370, 194
Mateo M. L., 1998, ARA&A 36, 435
Mathis J.S. 1990, ARA&A 28, 37
Nowotny W., Kerschbaum F., Olofsson H., Schwarz H. E., 2003, A&A, 403, 93
Osterbrock D. E., 1989, in Astrophysics of Gaseous Nebulae and Active Galactic Nuclei (Mill Valley: Univ. Science Books)
Peimbert M., Torres-Peimbert, S., 1983, IAU Symp. 103, Planetary Nebulae, ed. D. R. Flower (Kluwer, Dordrecht), p. 233
Perinotto M., Morbidelli L., Scatarzi A., 2004, MNRAS, 349, 793
Rauch T., 2003, A&A 403, 709
Richer M. G., 2006, to appear in the proceedings of the IAU symposium 234, April 3-6 2006, held in Hawaii
Richer M. G., & McCall M. L., 1995, ApJ, 445, 642
Richer M. G., Stasinska G., & McCall M. L., 1999, A&AS, 135, 203
Skillman E. D., Kennicutt R. C., Hodge P. W., 1989, ApJ, 347, 875
Schlegel, D. J., Finkbeiner, D. P., Davis, M., 1998, ApJ, 500, 525
Sohn Y.-J., Kang A., Rhee J., Shin M., Chun M.-S., & Kim Ho-Il, 2006, A&A, 445, 69
Stanghellini L., & Kaler J. B., 1989, ApJ 343, 811
Stasinska G., Richer M. G., McCall M. L., 1998, A&A, 336, 667
van Hoof P. A. M., Weingartner J. C., Martin P. G., Volk K., & Ferland G. J., 2004, MNRAS, 350, 1330
Van Zee L., Skillman E. D., Haynes M. P., 2006, ApJ, 637, 269
Vassiliadis E., & Wood P. R., 1994, ApJS, 92, 125
Young L. M., & Lo K. Y., 1997, ApJ, 476, 127
Zijlstra A. A., Gesicki K., Walsh J. R., Péquignot D., van Hoof P. A. M., Minniti D., 2006, MNRAS, 369, 875

Table 1. Observed emission-line fluxes, de-reddened intensities and CLOUDY modeled intensities

	PN1			PN2			PN3			PN4		
Ion	F	I	I_{CLOUDY}	F	I	I_{CLOUDY}	F	I	I_{CLOUDY}	F	I	I_{CLOUDY}
372.7 [O II]	<5.3	<5.3	15.0	<8.3	<8.5	30.	-	-	-	27.5	30.1	30.1
383.5 H9	-	-	-	-	-	-	-	-	-	4.5	4.9	7.3
386.8 [Ne III]	-	-	-	30.4	30.6	30.2	8.6	8.6	8.4	9.7	10.5	10.5
388.9 HeI, H8	-	-	-	-	-	-	73.6	73.6	-	8.5	9.2	10.5
396.7 [Ne III],H7	-	-	-	58.2	59.5	-	62.9	62.9	-	17.8	19.2	16.0
410.1 Hδ	-	-	-	-	-	-	-	-	-	23.6	25.1	26.0
434.0 Hγ	36.9	37.1	47.1	41.5	42.0	47.2	33.8	33.8	46.6	44.1	46.0	47.0
436.3 [O III]	11.5	11.6	9.5	17.4	17.6	16.0	16.0	16.0	15.5	1.5	1.6	3.7
447.1 HeI	-	-	-	-	-		-	-	-	4.0	4.1	7.9
468.6 HeII	<10	<11	16.6	3.5	3.5	4.9	14.1	14.1	13.4	1.7	1.7	1.8
486.1 Hβ	100.	100.	100.	100.	100	100	100.	100	100	100.	100.	100.
495.9 [O III]	244.4	244.1	235.1	308.3	307.6	291.0	255.4	255.4	242.1	120.4	119.5	121.4
500.7 [O III]	710.7	709.6	707.7	865.6	862.6	875.4	712.2	712.2	729.0	364.	359.8	365.3
575.5 [N II]	-	-	-	-	-	-	-	-	-	1.6	1.5	0.8
587.6 HeI	14.5	14.4	14.0	13.0	12.7	12.4	6.4	6.4	6.7	22.9	21.4	21.2
654.8 [N II]	-	-	-	-	-	-	-	-	-	17.4	15.8	15.1
656.3 Hα	288.9	285.0	278.6	293.6	285.0	274.0	260.	260.	258.	315.	285.	281.
658.4 [N II]	<6	<6	6.0	17.1	16.6	16.2	<1	<1	1.1	49.6	44.8	44.5
667.8 HeI	-	-	-	-	-		-	-	-	2.5	2.2	6.0
671.7 [S II]	<1.3	<1.2	1.2	-	-	-	-	-	-	1.4	1.3	1.3
673.1 [S II]	<2	<2	2.0	-	-	-	-	-	-	2.1	1.9	2.0
706.5 HeI	-	-	-	-	-	-	-	-	-	1.8	1.6	1.6
713.5 [Ar III]	-	-	-	1.3	1.2	1.3	1.	1.	1.1	1.6	1.4	1.5
728.1 HeI	-	-	-	-	-	-	-	-	-	0.5	0.5	0.6
732.0 [O II]	-	-	-	-	-	-	-	-	-	2.4	2.1	1.2*
733.0 [O II]	-	-	-	-	-	-	-	-	-	1.4	1.2	1.2*
906.9 [S III]	-	-	-	0.57	0.54	0.61	-	-	-	-	-	-
953.2 [S III]	-	-	-	-	-	-	<2	<2	0.3	-	-	-
c_β	0.02±0.003			0.04±0.01			0.0±0.02			0.14±0.02		

	PN6			PN7			PN10		
Ion	F	I	I_{CLOUDY}	F	I	I_{CLOUDY}	F	I	I_{CLOUDY}
372.7 [O II]	<35	<35	74.0	<5	<5	17.0	<65	<73	-
396.7 [Ne III],H7	-	-	-	21.6	22.7	16.0	-	-	-
410.1 Hδ	-	-	-	14.2	14.8	26.1	-	-	-
434.0 Hγ	-	-	-	34.3	35.3	47.0	-	-	-
436.3 [O III]	<12	<12	7.0	6.8	7.0	7.7	-	-	-
447.1 HeI	-	-	-	-	-	-	-	-	-
468.6 HeII	5.8	5.8	6.3	4.0	4.1	4.8	-	-	-
486.1 Hβ	100.	100.	100.	100.	100.	100.	100.	100	-
495.9 [O III]	186.9	186.9	216.2	257.8	256.5	253.	200.4	198.7	-
500.7 [O III]	659.5	659.5	650.1	788.3	782.0	761.5	627.8	619.7	-
575.5 [N II]	-	-	-	-	-	-	-	-	-
587.6 HeI	5.8	5.8	6.8	20.9	20.0	19.7	-	-	-
654.8 [N II]	41.1	41.1	36.3	-	-	-	24.2	21.7	-
656.3 Hα	284.2	284.2	280.0	304.9	285.	281.0	318.6	285.	-
658.4 [N II]	109.1	109.1	107.2	1.4	1.3	1.3	76.9	68.7	-
667.8 HeI	-	-	-	2.5	2.3	5.6	-	-	-
671.7 [S II]	6.0	6.0	5.9	-	-	-	22.7	20.2	-
673.1 [S II]	10.1	10.1	10.1	-	-	-	17.2	15.3	-
706.5 HeI	-	-	-	1.3	1.2	1.2	-	-	-
713.5 [Ar III]	4.6	4.6	4.5	1.	0.9	0.9	1.6	1.	-
c_β	0.0±0.02			0.1±0.04			0.16±0.05		

This paper has been typeset from a TEX/ LATEX file prepared by the author.

Table 2. Percentage errors in line fluxes (wrt $I_{H\beta}$=100)

Line Fluxes	PN1	PN2	PN3	PN4	PN6	PN7	PN10
1–5	27	30	26	23	35	25	37
5–15	22	26	20	17	28	23	29
15–30	18	22	16	14	23	15	25
30–200	12	17	12	10	15	11	21
200–500	07	11	06	05	08	06	15
500–1000	05	7	05	03	05	04	09

Table 3. Physical parameters and CLOUDY input parameters

Parameter	PN1		PN2		PN3		PN4	
	Empirical	CLOUDY	Empirical	CLOUDY	Empirical	CLOUDY	Empirical	CLOUDY
T_e[O III](K)	13800±2600	13300	15200±4000	15100	15900±2700	16300	9200±1400	12000
T_e[N II](K)	-	-	-	-	-	-	14900±3000	12000
T_e[O II](K)	-	-	-	-	-	-	16000±6000	-
N_e[S II](cm^{-3})	4700:	-	-	-	-	-	2800±600	3000
N_H(cm^{-3})	-	5300	-	5000	-	5000	-	2600
T$_\star$(K)	-	91300	-	75000	-	110000	-	70000
log(L$_\star$/L $_\odot$)	-	2.1	-	2.5	-	2.5	-	3.425
logR_{in} (cm)	-	11.9	-	12.	-	12.	-	12.
logR_{ext}(cm)	-	16.6	-	16.9	-	17.4	-	18.

Parameter	PN6		PN7		PN10	
	Empirical	CLOUDY	Empirical	CLOUDY	Empirical	CLOUDY
T_e[O III](K)	<14800	12000	12400±3600	12000	-	-
N_e[S II](cm^{-3})	5000±1800	-	-	-	100±35	-
N_H(cm^{-3})	-	5800	-	5000	-	-
T$_\star$(K)	-	84000	-	71000	-	-
log(L$_\star$/L $_\odot$)	-	1.8	-	3.275	-	-
logR_{in} (cm)	-	12.	-	12.	-	-
logR_{ext}(cm)	-	16.6	-	17.3	-	-

Table 4. ICF: ionic and total chemical abundances, and ionization correction factors

	PN1	PN2	PN3	PN4	PN6	PN7
$He^{+}/H^{+}\times10^{2}$	8.6±1.0	7.5±1.0	3.8±0.8	14.9±2.0	3.4±1.0	14.0±2.
$He^{++}/H^{+}\times10^{2}$	<0.88	0.3±0.1	1.2±0.5	0.2±0.1	0.5±0.2	0.4±0.2
$He/H\times10^{2}$	<9.44	7.8±1.1	5.0±1.3	15.1±2.1	3.9±1.2	14.4±2.2
12 +log(He/H)	<10.97	10.9±0.10	10.70±0.11	11.18±0.06	10.59±0.14	11.16±0.07
CLOUDY	<11.1	11.03±0.23	10.83±0.17	11.22±0.14	10.76±0.22	11.27±0.15
$O^{+}/H^{+}\times10^{7}$	<2.9	<4.4	-	57.±25.	<13.7	<5.0
$O^{++}/H^{+}\times10^{5}$	9.2±5.4	9.5±4.7	7.3±3.3	8.5±3.6	8.3±4.3	20.7±10.
ICF(O)	1.067	1.028	1.21	1.01	1.15	1.03
$O/H\times10^{5}$	9.8±6.	9.8±4.9	8.8±4.0	9.1±3.9	11.1±5.	21.3±10.
12 +log(O/H)	8.0±0.31	8.0±0.24	7.94±0.21	7.95±0.3	8.04±0.21	8.32±0.22
CLOUDY	8.12±0.13	8.00±0.16	8.10±0.12	7.98±0.14	8.28±0.14	8.16±0.12
$N^{+}/H^{+}\times10^{7}$	<2.3	6.6±3.7	0.4±0.4	52.±13.	150.±50.	2.3±2.
ICF(N)	<342	<222	-	15.9	<8.	<91.
$N/H\times10^{5}$	<7.8	<14.7	-	8.2±5.	<12.2	<2.1
12 +log(N/H)	<7.89	<8.16	-	7.91±0.3	<8.09	<7.3
CLOUDY	<7.4	7.59±0.25	<5.7	7.80±0.16	7.95±0.20	7.2±0.23
$Ne^{++}/H^{+}\times10^{6}$	-	6.1±3.0	1.9±1.0	6.4±2.9	-	-
ICF(Ne)	-	1.07	1.21	1.08	-	-
$Ne/H\times10^{6}$	-	7.4±3.0	2.3±1.9	6.9±5.3	-	-
12 +log(Ne/H)	-	6.87±0.20	6.36±0.51	6.83±0.30	-	-
CLOUDY	-	6.91±0.21	6.37±0.17	6.76±0.16	-	-
$S^{+}/H^{+}\times10^{8}$	<2.8	-	3.2±0.1	4.4±1.7	16.6± 2.	-
$S^{++}/H^{+}\times10^{7}$	-	-	-	-	-	0.3±0.2
ICF(S)	4.85	-	-	1.44	2.49	9.5
$S/H\times10^{7}$	<24.	-	-	6.3±2.3	44.±8.	11.7±3.
12 +log(S/H)	<6.38	-	-	5.80±0.14	6.64±0.10	6.06±0.11
CLOUDY	<6.56	<4.86	<4.28	5.79±0.22	6.54±0.26	<5.98
$Ar^{++}/H^{+}\times10^{7}$	-	0.3±0.2	0.3±0.2	1.0±0.3	1.2± 1.3	0.7± 0.4
ICF(Ar)	-	1.9	1.9	1.08	1.87	1.03
$Ar/H\times10^{7}$	-	0.6±0.5	0.6±0.5	1.05±0.6	2.3±2.6	0.7± 0.4
12 +log(Ar/H)		4.78±0.50	4.78±0.50	5.02±0.27	5.36±0.32	4.84±0.28
CLOUDY	-	4.86±0.27	4.86±0.23	5.07±0.21	5.51±0.26	4.96±0.23

Table 5. CLOUDY: total abundances. The abundances are given as 12+ log X/H.

	He/H	O/H	N/H	Ne/H	S/H	Ar/H
PN1	<11.1	8.12± 0.13	<7.4	-	<6.56	-
PN2	11.03± 0.23	8.05± 0.16	7.59± 0.25	6.91± 0.21	<4.86	4.86± 0.27
PN3	10.83± 0.17	8.10± 0.12	<5.7	6.37± 0.17	<4.28	4.86± 0.23
PN4	11.22± 0.14	7.98± 0.14	7.80± 0.16	6.76± 0.16	5.79± 0.22	5.07± 0.21
PN6	10.76± 0.22	8.28± 0.14	7.95 ± 0.20	-	6.54± 0.26	5.51± 0.26
PN7	11.21± 0.15	8.16± 0.12	7.20 ± 0.23	-	<5.98	5.01± 0.23
mean	$11.02^{+0.20}_{-0.36}$	$8.06^{+0.09}_{-0.12}$	$7.70^{+0.18}_{-0.31}$	$6.68^{+0.18}_{-0.32}$	$6.35^{+0.25}_{-0.68}$	$5.13^{+0.24}_{-0.64}$